

WILEY-VCH



European Chemical
Societies Publishing

Take Advantage and Publish Open Access



By publishing your paper open access, you'll be making it immediately freely available to anyone everywhere in the world.

That's maximum access and visibility worldwide with the same rigor of peer review you would expect from any high-quality journal.

Submit your paper today.



www.chemistry-europe.org

Impact of the Local Environment of Amines on the Activity for CO₂ Hydrogenation over Bifunctional Basic – Metallic Catalysts

Jakub Pazdera,^[a] Dilara Issayeva,^[b] Juliane Titus,^[b] Roger Gläser,^[b] Olaf Deutschmann,^[c] and Andreas Jentys^{*,[a]}

Bifunctional basic-metallic catalysts proved to be efficient for the selective hydrogenation of CO₂ to methanol. The activity of these catalysts depends on the cooperative interaction between the amine groups and metallic sites, which is a function of amine group density, Pd particle perimeter length and the geometric properties of support pores. The pore width has the

highest effect on the activity, increasing the methanol yield by about half an order of magnitude. Confining the space leads to a three-dimensional utilization of the available metal surface sites compared to a two-dimensional distribution of the bifunctional sites in larger pores, where the metal particle diameter is the decisive factor for the catalytic properties.

Introduction

Carbon capture processes are considered to be essential in order to establish a sustainable carbon neutral society.^[1] The majority of climate change predictions reach the conclusion that it will be impossible to restrict global warming without a large scale deployment of negative emission technologies.^[2] Reaction routes allowing to convert CO₂, removed by capture processes, to fuel components or base chemicals would increase the economic efficiency compared to CO₂ sequestration. One option is to use CO₂ from adsorptive capture as feed in conventional methanol synthesis. However, a more efficient approach is to combine CO₂ capture and conversion into a single, integrated process connecting adsorption and subsequent reactive regeneration. Several concepts were demonstrated over the last decade.^[3] One developed by Klankermayer

and Leitner et al.^[4] uses an alcohol as additive to form ester intermediates while the other, developed by Sanford,^[3a,5] Olah and Prakash^[3e] employs amines to form carbamates (R-NCOO⁻) and subsequently amides (R-NCHO). These additives provide a thermodynamic driving force to hydrogenate CO₂ and to overcome the primary barrier of the endergonic step of hydrogenating CO₂ to the formic acid level (i.e., carbamate).^[6]

Solid Pd-functionalized materials proved to be efficient catalysts for amine formylation to amides, i.e., hydrogenation of CO₂ to the aldehyde level.^[7] Kothandaram et al. used supported Pd-catalysts for amine assisted hydrogenation of CO₂ in condensed phases. Although achieving reasonable yields for amides, the Pd catalysts were unable to reduce the amides to methanol, but rather yielded methylated amines caused by a selective C–O bond cleavage.^[8] Studies on molecular hydrogenation catalysts revealed that a basic moiety close to the metal center is crucial for the selective C–N bond cleavage.^[9] This metal ligand cooperation facilitates heterolytic H₂ cleavage, which is highly beneficial for H₂ addition to carbonyl species. Additionally, the base acts as proton shuttle, transferring H from the O to the N atom of the hemiaminal intermediate, thereby retarding the C–O bond cleavage.^[9–10] Several studies on metal nanoparticles on basic supports showed that the interaction between the base and the metal particle results in heterolytic H₂ cleavage, accelerating carbonyl group hydrogenation and in changing the selectivity towards unsaturated bonds.^[11]

Only three heterogeneous systems for selective C–N bond cleavage were published.^[10a,12] The group of Milstein developed a system comprised of Ag particles on basic γ -Al₂O₃ that hydrogenates amides selectively via C–N bond cleavage. The interaction of the basic support and the metal particles proved to be crucial for the reaction facilitating heterolytic H₂ cleavage.^[10a,13] Kar et al. explored the use of solid supported sorbents, which can be easily separated and reused, but to this date solid catalyst systems that combine basic CO₂ capture sites

[a] J. Pazdera, Prof. A. Jentys
Technical University of Munich
Department of Chemistry
Catalysis Research Center
Garching 85747 (Germany)
E-mail: jentys@tum.de

[b] D. Issayeva, Dr. J. Titus, Prof. R. Gläser.
Institute of Chemical Technology
Universität Leipzig
Leipzig 04103 (Germany)

[c] Prof. O. Deutschmann
Institute for Chemical Technology and Polymer Chemistry
Karlsruhe Institute of Technology
Karlsruhe 76131 (Germany)

 Supporting information for this article is available on the WWW under <https://doi.org/10.1002/cctc.202200620>

 This publication is part of a joint Special Collection with ChemElectroChem on "Catalysts and Reactors under Dynamic Conditions for Energy Storage and Conversion (DynaKat)". Please check our homepage for more articles in the collection.

 © 2022 The Authors. ChemCatChem published by Wiley-VCH GmbH. This is an open access article under the terms of the Creative Commons Attribution Non-Commercial NoDerivs License, which permits use and distribution in any medium, provided the original work is properly cited, the use is non-commercial and no modifications or adaptations are made.

with metal-based hydrogenation sites in a single material were not published.^[3d]

In our previous work, we showed that Pd – amine functionalized silica can bind and selectively convert CO₂ to methanol. The reaction proceeds via a carbamate formed upon reaction of two amines with one CO₂ molecule and the corresponding formamide, formed by the reaction of the carbamate with H₂. In the last step the formamide undergoes selective hydrogenolysis yielding methanol, while recovering the primary amine.^[14]

In this work we present an integrated solid sorbent and catalyst, which adsorbs and selectively converts CO₂ to methanol and focus on the effect of structural and electronic properties on the activity of this material.

Results and Discussion

Characterization

The synthesis method applied allows to adjust the Pd content of the catalyst over a wide range by controlling the Pd concentration in the precursor solution (Figure 1a). Higher Pd loadings lead to consistently higher amine loadings (Figure 1b), indicating the preferential anchoring of the amines at the circumference of the metal particles (which is confirmed by XPS measurements (Figure 10d) and discussed later). The BET surface area (Figure 1c) of the catalyst decreased significantly after grafting amines onto the surface, which resulted from pore blockage of smaller pores (micropore volume of the calcined material is lost entirely) as well as from the occupation of space on the surface support.^[15]

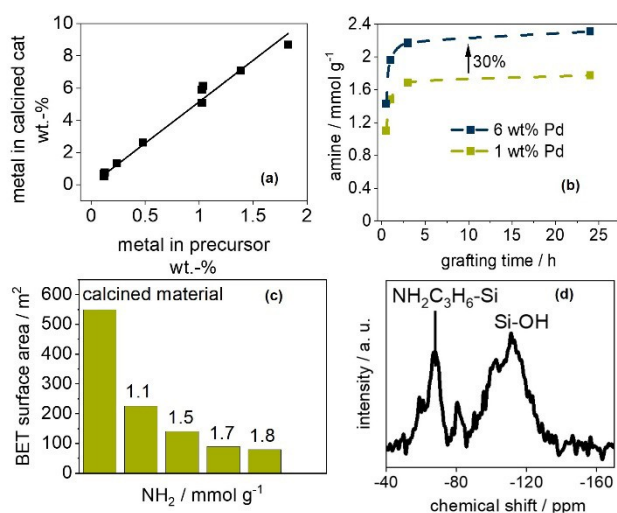


Figure 1. (a) Metal loading in the final catalyst scales linearly with the metal content in the precursor solution used for the sol-gel synthesis. (b) Amine content increases with the Pd loading of the catalyst precursor. (c) BET surface area (1 wt.-% Pd) decreases with increasing amine loading due to pore blockage and occupation of the surface. (d) ²⁹Si MAS NMR confirms the covalent bond of the propylamine to Si-OH groups.

The formation of covalent bonds between the aminosilane and the silica surface is confirmed by ²⁹Si (MAS) NMR (Figure 1d).

TEM micrographs show that the direct incorporation during the sol-gel process yields relatively large Pd particles with a broad size distribution that are evenly distributed on the support (Figure 2).

Catalytic activity

The typical course of the most significant masses recorded during the reaction with an on – line mass spectrometer is shown in Figure 3. During the last step of the cycle, the temperature was increased from 343 K to 413 K, which led to the desorption of strongly bound CO₂ followed by methanol and water as products. Other products such as CO or CH₄ were not observed within the detection limits.^[14] The reaction showed a stable activity of the catalyst for 9 consecutive cycles (SI Figure 7). Additionally, X-ray absorption spectroscopy

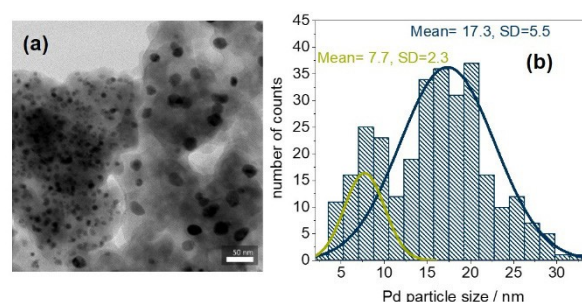


Figure 2. (a) TEM image of a bifunctional catalyst. (b) Pd particle size distribution of Si/Pd(6.0)-NH₂.

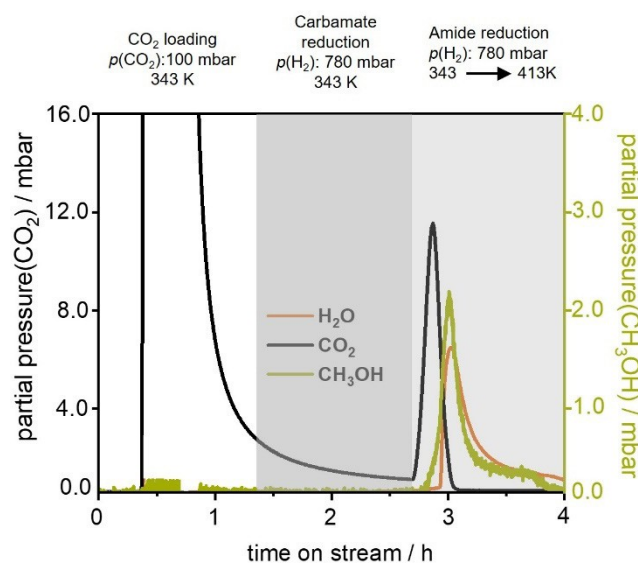


Figure 3. Reaction sequence used to study the catalytic activity of the materials. Measured ion currents are converted to partial pressures using prior determined response factors.

Table 1. Bifunctional amine-metal-catalysts investigated for their CO₂ hydrogenation activity. For each group I–III one parameter (dark grey) was varied, and the influence on the activity was studied.

No.	Sample	N [mmol g ⁻¹]	BET [m ²]	Amine density [NH ₂ nm ⁻²]	Pd [wt.-%]	Median pore diameter [nm]	
I	1	Si/Pd-NH ₂ (1.1)	1.1	226	2.9	6.0	17.3
	2	Si/Pd-NH ₂ (1.4)	1.4	137	6.1	6.0	19.8
	3	Si/Pd-NH ₂ (1.7)	1.7	85	12.0	6.0	20.4
II	4	Si/Pd(1.5)-NH ₂	1.7	89	11.5	1.5	19.8
	5	Si/Pd(3.0)-NH ₂	1.6	83	11.6	3.0	19.6
	6	Si/Pd(6.0)-NH ₂	1.7	85	12.0	6.0	20.4
III	7	Si(5.7)/Pd-NH ₂	1.0	341	1.8	3.1	5.7
	8	Si(8.0)/Pd-NH ₂	1.1	281	2.3	3.0	8.0
	9	Si(9.5)/Pd-NH ₂	1.1	302	2.1	3.0	9.5
	10	Si(12)/Pd-NH ₂	1.1	221	2.7	3.2	12.0

showed that the catalyst is stable under the reaction conditions (see S4 & S5).

A series of bifunctional basic-metallic catalysts with varying amine and metal loadings as well as pore diameters were synthesized to study the influence of the metal-amine-interface on the activity (Table 1).

In every group of materials (I–III) one parameter was varied (highlighted in dark grey), while the others were kept constant. Please note that the materials of group I and II exhibit a hierarchical pore structure with a broad distribution of pore widths, hence, the influence of the pore structure cannot be assessed from these samples. Therefore, SBA-15 with defined pore width was used as a support for group III of materials. Details of the synthesis procedures can be found in the experimental section.

For materials of group I we used the same Pd loaded silica catalyst and varied the amine density. The CO₂ sorption capacity and the total methanol yield per cycle increased significantly with increasing amine loading (Figure 4b). By increasing the amine loading from 1.1 to 1.7 mmol g⁻¹, a fourfold increase in the CO₂ capacity was observed. This resulted in a twofold rise of the methanol yield, while the conversion based on the overall CO₂ adsorption capacity decreased with increasing amine loading (Figure 4a). This indicates that the majority of the sites available for grafting of the amines at the metal circumference were already occupied at lower amine loadings, while the additional amines were grafted at positions on the support without direct contact to the metal. Hence, the CO₂ adsorption capacity was enhanced due to the presence of additional amine groups on the surface, but the CO₂ molecules were not hydrogenated due to the absence of H formed on the metallic sites by dissociative adsorption of H₂. This trend confirms the hypothesis that sites at the metal circumference are preferred during the amine grafting and are occupied first (see Figure 1a). Therefore, an increased amine loading can only increase the activity if the number of available sites at the Pd particle perimeter is also increased during the synthesis.

For group II of materials the amine content was kept constant and the metal loading was varied (Table 1). The CO₂ conversion increased with the metal loading, however, the effect was rather small (Figure 5) as the particle size of the metal clusters increased simultaneously (SI Figure 1). As we

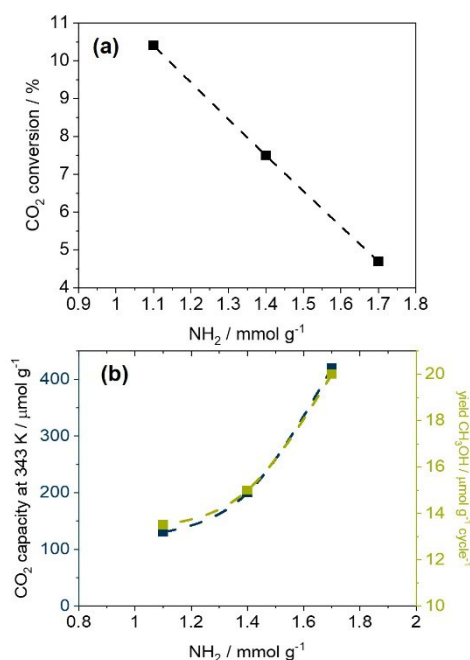


Figure 4. (a) CO₂ conversion, based on the total CO₂ adsorption capacity (determined by TGA) at 343 K as a function of amine loading (1 wt.-% Pd). (b) CO₂ adsorption capacity and methanol yield as a function of amine loading.

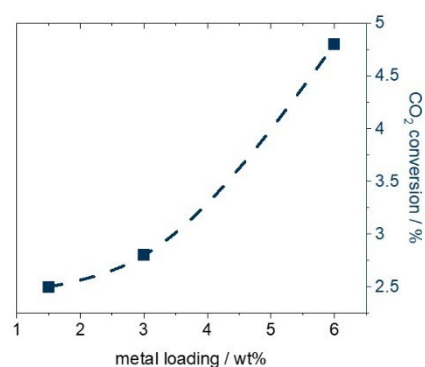


Figure 5. CO₂ conversion (based on total CO₂ adsorption capacity at *p*(CO₂) = 100 mbar and *T* = 343 K determined with TGA).

assume that the reaction occurs only at the interface between the Pd particles and the amines grafted to the silica support, the total perimeter of all particles should be the crucial factor determining the activity. Calculations show that decreasing the particle size is a more efficient way to increase the perimeter than increasing the Pd loading (SI Figure 3).

The selectivity to methanol was, as expected, not affected by the particle size, as we assume that the reaction takes place at the interface between Pd and amine. Therefore, the pathway of the reaction is only controlled by the formation of the reaction intermediates on amine (as discussed below).

Group III of the materials was prepared to examine the influence of the pore width on the activity. For a precise control over the pore width we first synthesized a series of SBA-15 supports using hydrothermal synthesis^[16] and varied the pore width by adjusting the duration of the hydrothermal treatment.^[17] All materials in this group showed an almost complete conversion of irreversibly bound CO₂ (95–98%), indicating that on these materials all amine sites were in direct contact with a metal particles. The CO₂ adsorption capacity and amine efficiency (adsorbed CO₂/NH₂, maximum = 0.5, since two

amine groups are necessary to bind one CO₂ molecule^[15b,18]) were very low on these materials due to the low amine loading. At 343 K only 70 μmol/g CO₂ were adsorbed, however, the material (Si(5.7)/Pd-NH₂) yields 22 μmol/g methanol per cycle by converting 31 % of the adsorbed CO₂.

The methanol yield as a function of the pore width is shown in Figure 6. A smaller pore width resulted in a higher methanol yield, which indicates that in materials with small pores CO₂ adsorbed on amine groups present around the metal particles can be converted. In contrast, for materials with larger pores CO₂ can only be converted if adsorbed on amine groups at the perimeter (see Scheme 1).

These results reveal that the activity is not determined by the absolute number of amine and/or metal sites, but only by the fraction of sites present at the metal-amine interface. When the pore width is significantly larger than the length of the propylamine chain, the perimeter of the metal and the amine density appear to be significant as only the two-dimensional perimeter can be utilized. With decreasing pore width, the surface amine density becomes less important and, due to the curvature of the pore, amine groups from the adjacent side of the pore are in contact with the metal surface and thus can act as additional active sites for binding and converting CO₂ to methanol. Therefore, the entire surface of the metal particle can be utilized resulting in an enhanced methanol yield (Figure 6).

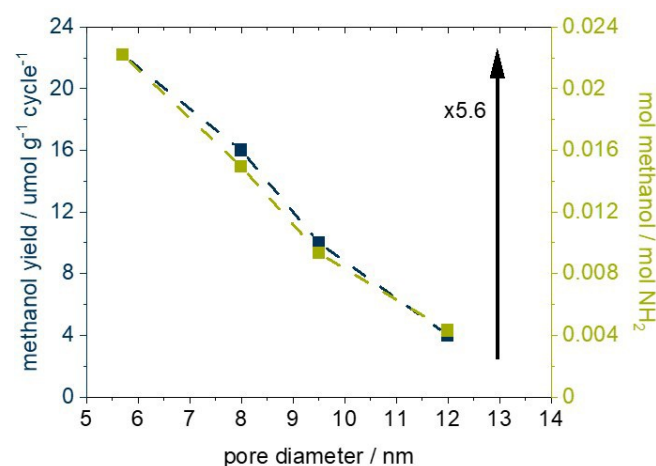
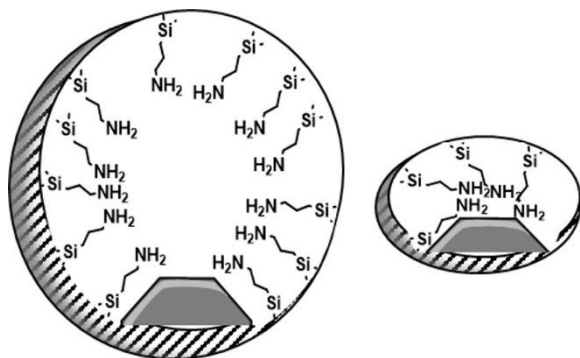


Figure 6. Methanol yield (blue) and methanol yield per amine group (green) as a function of pore width.



Scheme 1. Decreasing the pore diameter (at constant amine loading and density) brings amine groups and metal particles closer together, thereby increasing the available interface for the reaction.

CO₂ adsorption properties

Surface species present under reaction conditions were investigated by IR spectroscopy to distinguish reactive and unreactive CO₂ adsorption sites. Experimental and theoretical publications have shown that CO₂ adsorption (i.e., physisorbed CO₂ and various types of chemisorbed CO₂) depends on the amine density, the partial pressure of CO₂ and the sorption temperature.^[18a,19] The properties of the materials selected to study the influence of the amine group density and the functionalization with Pd on the CO₂ adsorption are summarized in Table 2. CO₂ chemisorption on primary amines proceeds via the formation of carbamates and/or carbamic acid.^[15b,18–19,20] IR-spectra during the adsorption of CO₂ (Figure 9) show that carbamate formation is favored under conditions typical for post combustion capture ($p(\text{CO}_2) = 100 \text{ mbar}$, 343 K). The formation of carbamates requires two amines in proximity and results in a maximum amine-efficiency of 0.5, i.e., one molecule of CO₂ is bound to two –NH₂ groups.

Table 2. Materials used to study the effect of different amine densities on the CO₂ adsorption behavior. Numbers in parenthesis denote the amine density of the sample.

Sample	NH ₂ [mmol g ⁻¹]	BET [m ²]	Amine density [NH ₂ nm ⁻²]
Si-NH ₂ (3.3)	2.5	421	3.3
Si-NH ₂ (7.2)	3.5	290	7.2
Si-NH ₂ (15.7)	4.7	182	15.7
Si/Pd-NH ₂ (12.0)	1.7	85	12.0

The amine efficiency as function of amine density and temperature is shown in Figure 7. The amine efficiency strongly depends on the amine density and, therefore, it is expected to determine the activity of the catalyst.

The adsorption isotherms of CO₂ recorded at 343 K and 363 K are shown in Figure 8a. The uptake at 343 K can be described with a dual-Langmuir isotherm, revealing the additional contribution of physisorption. At higher temperatures the experimental data can be fitted with a single Langmuir isotherm, indicating that chemisorption dominates with increasing temperature. With increasing local amine density an additional stabilization of chemisorbed CO₂ may occur via hydrogen bonding to neighboring amines.^[18b]

The heterogeneity of the adsorption sites is reflected by the decrease in the differential adsorption enthalpies from an initial

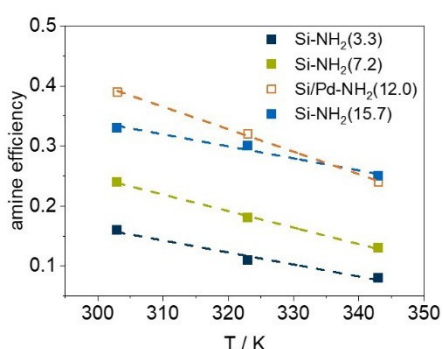


Figure 7. Amine efficiency for materials with different amine densities as a function of temperature.

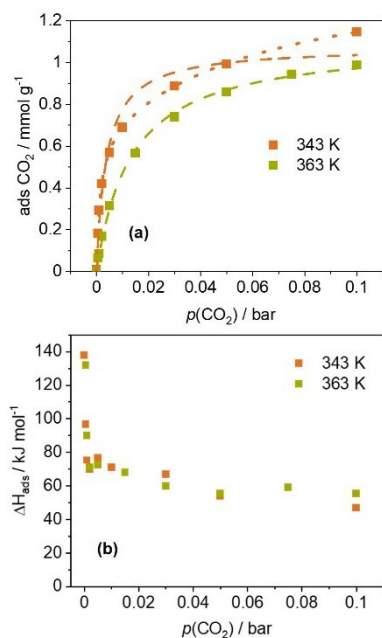


Figure 8. (a) CO₂ adsorption isotherm of Si - NH₂(15.7). Experimental data were fitted with a Langmuir and Dual-Langmuir (dotted line) (343 and 363 K) model. (b) Differential heat of adsorption obtained during measurement of the isotherms.

value of 140 kJ mol⁻¹ to around 60 kJ mol⁻¹ with increasing CO₂ coverage (Figure 8b).^[21]

IR spectroscopy revealed that the ratio between carbamates and carbamic acid formed depends on the partial pressure of CO₂, as higher pressure favors carbamic acid formation and on the amine density (see Figure 9, detailed band assignments can be found in the SI table S1 & table S2). High amine density (Figure 9a) resulted in a lower formation of carbamic acid (1697 cm⁻¹). This shows that CO₂ adsorbs in various configurations on the surface and different degrees of stabilization, which will influence the reactivity of the adsorbed species. While detailed correlations remain to be investigated, these results indicate that the density of sites and their interaction as well as the external conditions affect the nature of adsorbed species and thus the reactivity of the catalyst.

Electronic properties of Pd

The electronic interaction between the Pd particles and amines on the surface was studied by XPS. The Pd 3d_{5/2} and 3d_{3/2} spectra of PdO, Pd⁰ and Pd⁰-NH₂ are compared in Figure 10a. The binding energies (BE) of the 3d_{5/2} and 3d_{3/2} levels of PdO and Pd⁰ match the values reported in literature,^[22] generally shifting to lower BE with lower oxidation state. The BE of the amine functionalized catalyst Pd⁰-NH₂ decreased by 0.9 eV relative to Pd⁰, indicating a charge transfer from the amine to the Pd-particles.^[23] The charge transfer was additionally confirmed by IR-spectra of adsorbed CO on Pd, showing a shift to lower wavenumbers on amine functionalized Pd (SI Figure 6). Electron density donation to the Pd from a neighboring species was demonstrated to enhance the N-formylation activity of Pd.^[7f] The N 1s XPS of Pd and amine functionalized materials (Figure 10b) showed a broadening of the peak relative to the Si-NH₂ sample. Deconvolution of the N 1s peak reveals that the peak is comprised of two contributions at 399.1 eV and 400.6 eV (SI Figure 2). The first one is attributed to NH₂ and the latter to electron deficient NH₂, i.e., hydrogen bonded NH₂, NH₃⁺ or NH₂ interacting with Pd.^[24] Peak fitting indicated that the peak broadening is caused by a change of the relative

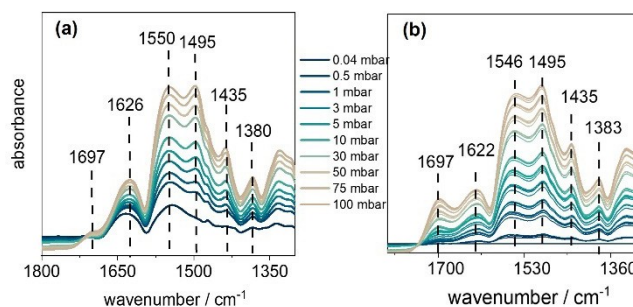


Figure 9. IR – spectra of CO₂ adsorption isotherm on amine functionalized silica. At low pressures carbamates (1626, 1550, 1495, 1435 cm⁻¹) are the dominating species, whereas at higher pressures carbamic acid is increasingly formed (1693 cm⁻¹). (a) Difference spectra of CO₂ adsorption on Si-NH₂(15.7). (b) Difference spectra of CO₂ adsorption on Si-NH₂(3.3).

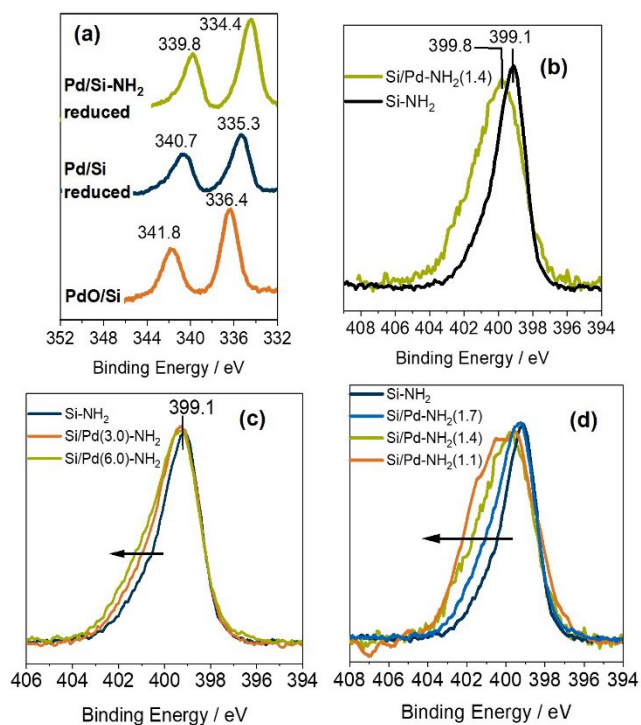


Figure 10. XPS of Pd and Pd-NH₂ materials. (a) Pd 3d spectra show a shift to lower binding energies with increasing electron density at the metal. (b) N 1s region spectra. Pd loading (sample Si/Pd-NH₂(1.4)) results in a broadening of the peak, caused by a changing ratio of the underlying peaks. (c) The peak broadening increases with increasing metal loading. (d) Lowering the amine loading at constant metal loading results in significant broadening of the peaks, which means that at lower amine loading, a higher fraction of the amines are interacting with the metal.

intensity of the peak at higher BE (400.6 eV), confirming that the amines interact with Pd and donate electron density to the metal (SI Figure 2).

The ratio between the peaks at 399.1 eV and 400.6 eV was used for a quantitative determination of the fraction of amine groups in direct contact to Pd. Peak deconvolution of the XPS of Si-NH₂ and Si/Pd(6.0)-NH₂ shows a relative contribution for the peak at 400.6 eV of 23.6% and 47.5%, respectively, which indicates that 23.9% of amines are located at the perimeter of the Pd particles. Since the amine efficiency for the CO₂ sorption on this sample was 0.25, around 6% of the adsorbed CO₂ was bound to basic sites in close proximity to Pd and thus can be converted to methanol. It should be noted that this value is in agreement with the conversion observed on this material, which was ~5% (Figure 4). Increasing the metal loading at constant amine loading resulted in an increase in the contribution of the peak at higher BE (Figure 10c), indicating a higher fraction of amines present at the NH₂-Pd interface. Deconvolution of the peaks (SI Figure 2) revealed an increase of the NH₂-Pd interface of 2.3% from Si/Pd(3.0)-NH₂ to Si/Pd(6.0)-NH₂, which is in agreement with the relative increase in activity observed for these samples (Figure 3). Figure 11 shows the CO₂ conversion as function of the area of the XPS peak at 400.6 eV, which is attributed to amines in direct contact with Pd particles

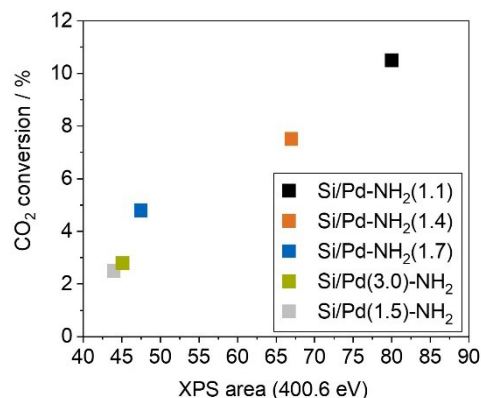


Figure 11. CO₂ conversion (based on total CO₂ adsorption capacity) as a function of the area of the XPS peak at 400.6 eV, which is attributed to amines in direct contact with Pd nanoparticles.

being active for the cooperative CO₂ conversion (Deconvolution of XPS can be found in the SI Figure 2).

Decreasing the amine loading resulted in a significant broadening of the peak, indicating that a larger fraction of amines is located at the Pd perimeter at lower loadings. This is in accordance with the reactivity observed (Figure 4a) and additionally supports the hypothesis that sites at the Pd perimeter are preferential grafting sites (Figure 1b).

Spectroscopic investigation of surface species (Amide hydrogenolysis)

It is commonly accepted that amine-assisted CO₂ conversion to methanol proceeds via an amide intermediate,^[3c,g,i,9] which was demonstrated previously by in situ IR spectroscopy on this catalyst system.^[15] CO₂ was adsorbed as carbamate and carbamic acid was hydrogenated to the corresponding amide in the first step and followed by the selective hydrogenolysis to methanol and the primary amine in the second step. As amides exhibit a high stability on the surface, amide functionalized catalysts were used to investigate the selectivity of the hydrogenolysis step (being the r.d.s.) in detail.

We hypothesize that only amide species interacting with a metal particle can be reduced, thus, in presence of H₂ there should be a limited number of amide species being converted to methanol. The time resolved IR spectra obtained during hydrogenolysis of amide functionalized Pd/Si are shown in Figure 12. The decrease of the amide I and II bands at 1683 cm⁻¹ and 1512 cm⁻¹ was accompanied by an increase of a band at 1594 cm⁻¹, attributed to the deformation vibration of primary amine NH₂ groups. The C-H stretching region was unaffected, indicating that the cleavage of the propyl group or the formation of methylated amine did not occur. Therefore, we can assume that the decrease of the amide bands resulted exclusively from the C-N bond cleavage leading to the formation of methanol. Comparing the areas of the amide I band before and after the reaction reveals that around 18% of

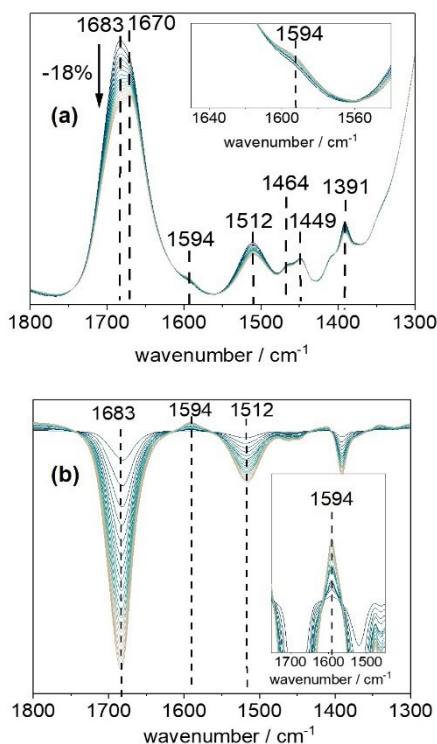


Figure 12. Time resolved IR- spectra of the hydrogenolysis of N-propylformamide grafted onto a Pd loaded silica at 413 K. (a) Absorbance spectra. (b) Difference spectra relative to the first spectrum of the reduction. The inserts show the increase of the NH_2 -deformation band of the primary amine at 1594 cm^{-1} .

the amide present on the surface was reduced, which is consistent with the estimation from the XPS that around 25% of the amines are close enough to a Pd particle in order to exhibit electronic interactions. These results additionally support our hypothesis, that the reaction takes place exclusively on the Pd-amine interface. The detailed mechanism resulting in the selective C–N bond cleavage is still under investigation. Suarez et al. demonstrated that selective C–N bond cleavage in amides by Noyori-type catalysts results from a transition state stabilization (i.e. stabilization of the hemiaminal) by either the amine ligand of the catalyst or by another amide molecule from the substrate.^[9] Note that heterolytic H_2 cleavage favors the selective hydrogenolysis.^[25] Recent work by Martinez-Prieto et al. demonstrated the heterolytic H_2 cleavage at the Ru- NH_2 interface of Ru nanoparticles supported on N doped graphene oxide^[11a] yielded a H^- on the metal and H^+ at the base. Wang et al. showed heterolytic cleavage between unsupported Pd and various nitrogen containing bases.^[26] Detailed mechanistic investigations on the Pd- NH_2 system used in this work are currently ongoing.

Conclusions

The present work demonstrates that the efficient CO_2 sorption and catalytic hydrogenation to methanol can be combined with one (bifunctional) material containing basic and metallic sites. The catalytic activity of the bifunctional catalysts for CO_2 reduction to methanol strongly depends on the local environment around the catalytic site. The presence of two cooperatively acting sites (amine and metal) on the surface is not sufficient to achieve a high activity. Instead, the local arrangement of the sites is essential for CO_2 adsorption, where amine density determines the amine efficiency i.e., the maximum of potentially convertible CO_2 and the chemical nature of adsorbed CO_2 . Providing a more confined space leads to an almost four times higher methanol yield in the subsequent CO_2 hydrogenation. With large pores, the amine-Pd interface is limited to the two-dimensional space at the particle perimeter. Decreasing the pore width enables the three-dimensional usage of the pore volume resulting in a high amine utilization despite low amine surface densities.

Experimental Section

Chemicals

(3-aminopropyl)trimethoxysilane (APTMS, Sigma-Aldrich, 97% purity), phenyltrimethoxysilane (PTMS, Sigma-Aldrich, 95% purity) and tetraethylorthosilicate (TES40, Wacker, 40% SiO_2) were used as sol-gel precursors. A propylene oxide/ethylene oxide block copolymer ((PO)₁₁(EO)₂₇(PO)₁₁, Pluronic RPE1740, BASF), benzyl alcohol (Merck, 99% purity) and palladium acetylacetonate (Sigma-Aldrich, 99% purity) were used for catalyst synthesis. (3-aminopropyl)trimethoxysilane (APTMS, Sigma-Aldrich, 97% purity) was used for grafting in anhydrous toluene (Sigma-Aldrich, 99.8%) as solvent. De-ionized water, ethanol (technical grade), isopropanol (technical grade) and toluene (technical grade) were used for washing of the final materials. (3-aminopropyl)trimethoxysilane (APTMS, Sigma-Aldrich, 97% purity) and methyl formate (Merck, 97% purity) were used for the synthesis of N-(3-trimethoxysilylpropyl) formamide. All chemicals were used as obtained without further purification.

Catalyst preparation

Materials of Group I & II

A mixture of 4.1 g RPE1740, 2.7 g Benzyl alcohol (24.97 mmol) and a variable amount of $\text{Pd}(\text{acac})_2$ was prepared and vigorously stirred for at least 40 min. In parallel, a mixture of 4.1 g APTMS (22.87 mmol), 1.5 g PTMS (7.56 mmol) and 2.1 g TES40 was prepared and stirred for 10 min. After stirring for the appropriate 1 h both components were mixed and blended together for another 10 min. The resulting mixture was injected into a water filled reactor column, where solid spheres were formed. The particles were washed with water immediately afterwards to remove any precursor left. The spheres produced in this process were kept in water for at least two days to ensure that the siloxane precursors remaining inside the particle were completely hydrolyzed. Afterwards, the materials were washed with water ($3 \times 100\text{ mL}$) and ethanol ($3 \times 100\text{ mL}$). The particles were pre-dried at

100 °C for at least 3 h and calcined at 550 °C for 4 h using a stream of 100 mL min⁻¹ of synthetic air.

Amine functionalization was done by grafting with a 1:1 vol.-% mixture of a trimethoxysilane modified amine and anhydrous toluene. The amine content was controlled by the grafting procedure. After grafting, the particles are washed with ethanol (1 × 100 mL–150 mL), iso-propanol (1 × 100 mL–150 mL) and toluene (1 × 50 mL–100 mL) are subsequently dried in vacuum at room temperature for 30 min and at 393 K for 3 h.

Catalysts with controlled pore size (Group III)

SBA-15, was synthesized in a cooperative self-assembly process. The template (surfactant), a non-ionic triblock copolymer (Pluronic P-123 obtained from BASF), was dissolved in 1 M HCl for four hours at 40 °C. Next, TEOS (obtained from Wacker) was added slowly to the mixture (mass ratio of TEOS/P123=2) and the stirring was continued for another two hours. The mixture was subsequently transferred to an autoclave, where a hydrothermal synthesis was carried out at 120 °C for reaction times between 16 and 66 hours.

The mixture was filtered, washed with deionised water and dried for 20 to 68 hours at a temperature 120 °C. The obtained powder was calcined at 450 °C for 4 h in 100 mL min⁻¹ synthetic air.

For the Pd impregnation the silica was stirred in deionised water. The pH was increased to 8 by addition of concentrated NH₄OH. The desired amount of palladium salt (PdAcAc) was dissolved in 5 mL of deionised water and then added to the silica slurry. The mixture kept stirring for one hour at room temperature. Next, the mixture was filtered and washed with water. The residue was then collected and dried for 20 hours at 120 °C. The samples were subsequently calcined at 450 °C for 4 h in 100 mL synthetic air.

Elemental composition

The carbon, hydrogen and nitrogen content of samples was determined using a HEKAtech Euro EA Elemental Analyzer. Samples were oxidized at 2073 K, the combustion gasses were chromatographically separated and detected using a TCD detector. Atomic absorption spectroscopy (AAS) was used to determine the Pd-content in the samples using a Solaar M5 Dual Flame graphite furnace AAS spectrometer from ThermoFisher. For analysis, 50–80 mg of the sample was dissolved in hydrofluoric acid, which was subsequently evaporated and the solid residue was dissolved in sulfuric acid and analyzed.

BET Analysis

The sample was activated in vacuum at 433 K for 4 h and then cooled to 77 K where N₂ adsorption was carried out with a Sorptomatic instrument. Mesopore volume and area were determined with the BJH-method on the desorption branch in a range of $p/p_0=0.25$ to 0.95 using the universal Harkins-Jura-isotherm defined in the ASTM D4641-87 standard. A t-plot was obtained by converting the data using the de Boer isotherm and the micropore volume was determined through a linear regression in the range of $t=0.6$ nm to 0.8 nm

²⁹Si MAS NMR

²⁹Si MAS NMR spectrum of the catalyst was acquired at a Bruker DRX-400 WB spectrometer (Bruker Biospin, Karlsruhe, Germany) equipped with a 4 mm MAS BB/1H probe operating at Larmor frequencies of 79.49 MHz and 400.15 MHz for ²⁹Si and ¹H,

respectively. Tetramethylsilane was used as an external reference. The speed of spinning was set to 12 kHz and a recycle delay time of 60 s was applied. A single-pulse direct excitation on ²⁹Si was used, 1024 scans were accumulated at a radio frequency of 42 kHz as a $\pi/2$ pulse. During the acquisition, proton decoupling was applied using SW_F-TPPM scheme at the radio frequency of 100 kHz.

XPS

X-ray photoelectron spectra (XPS) data were collected with a Kratos Axis Supra spectrometer at a base pressure <10⁻⁸ torr using monochromatic Al K_α radiation (E=1486.6 eV), a charge neutralizer, and pass energies of 160 eV (survey spectra) and 80 eV (region spectra). The binding energy was calibrated using the 1 s photoemission peak for adventitious carbon at 284.8 eV. Data analysis and modelling were performed with Origin using a Shirley background and Voigt line shapes.

CO₂ Adsorption

CO₂ adsorption measurements were carried out at ambient pressure and under flow conditions in a Setaram SENSYS Evo TG-DSC. The samples were activated in N₂ for 4 h at 433 K with a flow of 175 mL min⁻¹. CO₂-adsorption isobars were measured after saturating the samples in a stream of diluted CO₂ (10% CO₂ in N₂, 188 mL min⁻¹) and purging with 175 mL min⁻¹ N₂ for 5 h. At the desired temperature the gas flow was switched between CO₂ and N₂ during the cycle experiments. The sorption kinetics was followed by isothermal CO₂ adsorption at 303, 323 and 343 K and a CO₂ partial pressure of 100 mbar.

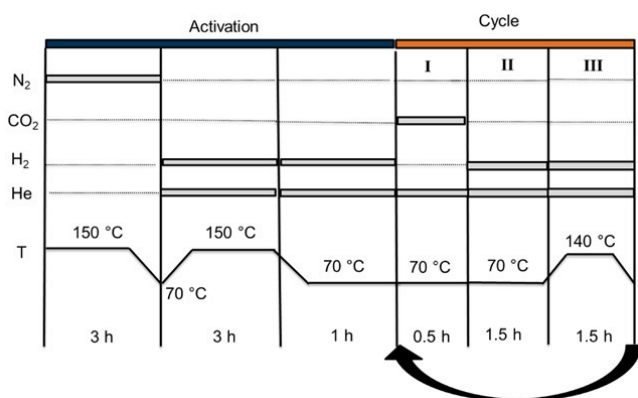
Adsorption isotherms were measured in a modified Setaram TG-DSC 111 balance attached to a vacuum system. The samples were activated for 4 h at 433 K in vacuum (10⁻⁶ mbar) and cooled to 343 K. The CO₂ was dosed into the system until a predefined pressure was reached and equilibration of the sorption process was established (after approx. 30 min for each pressure step). During this process, the mass of the sample and the heat flow were recorded every 2 s.

Catalytic activity

The catalytic activity was measured using a fixed-bed tubular reactor at 1 bar and temperatures between 343 K and 413 K, applying dynamic changes in the reactant feed in order simulate the periodic operation of a CO₂ (pressure-swing) absorber. CO₂ adsorption was carried out with 10% CO₂ in He at 343 K, followed (after purging with He) by hydrogenation using 78% H₂ in He at the sorption temperature for 120–210 min and by a linear temperature increase (5 K min⁻¹) to 413 K.

The cycle for the catalytic experiments is shown in Scheme 2. The species desorbing from the catalyst were detected with an OmniStar mass spectrometer from Pfeiffer Vacuum. For the quantitative evaluation of the mass spectra a calibration was performed for H₂, CO₂, CH₃OH and H₂O relative to He (internal reference) by feeding the gasses with 4–5 different partial pressures for each compound

The temperature for the CO₂ loading step was selected to be typical for the temperature of the flue gas after the desulphurization unit in a commercial coal fired power plant.^[27] Although methanol formation was already observed at temperatures as low as 363 K, it was necessary to increase the temperature to completely remove methanol from the catalyst.



Scheme 2. Experimental conditions used for activation and catalytic cycles. Typically, 10 sorption/reaction cycles were carried out in each experiment

IR – spectroscopy

In situ infrared spectroscopy was carried out in a Thermo Fisher Nicolet iS50 FT-IT spectrometer equipped with a vacuum cell. This cell is designed for transmission measurements and has CaF_2 windows. It is equipped with a heated sample holder in which a self-supporting wafer pressed from pulverized material can be placed. Prior to experiments, samples were activated for 4 h at 433 K in vacuum (10^{-6} mbar) and cooled to the temperature for adsorption while still in high vacuum. In the next step, the adsorbate was dosed into the system and IR spectra were collected until the sorption equilibrium was reached at the predefined pressure.

TEM

Transmission electron microscopy (TEM) analysis was performed at a JEM-2100Plus instrument (Jeol) operated at an accelerating voltage of 200 kV. The TEM is equipped with a LaB_6 cathode and high-resolution pole piece. The images were recorded with a 4 K CMOS camera (TVIPS) and EDX analysis was done by Octane T Optima (EDAX) windowless silicon drift detector. Sample preparation for TEM was performed by grinding in ethanol (99.5%, VWR). The dispersed particles were supported on a holey carbon Cu-TEM grid.

XAS

X-ray absorption spectroscopy (XAS) measurements were performed at the P65 beamline of the German electron synchrotron (DESY) in Hamburg, Germany.^[28] The PETRA III storage ring operated at 6 GeV energy and 100 mA beam current in top-up mode. A water-cooled Si311 double crystal monochromator (DCM) was used for obtaining monochromatic X-rays. Two Rh-coated plane mirrors were installed in front of the DCM to reject higher harmonics. The DCM was calibrated for Pd K-edge measurements by measuring a Pd-foil and setting the first inflection point to 24350 eV. A Pd foil was placed between the second and third ionization chamber for the energy calibration of each measured spectrum. The data were monitored for any signs of X-ray beam damage and several successive scans were averaged to reduce signal-to-noise ratio and improve the data quality. X-ray absorption near edge structure (XANES) and extended X-ray absorption fine structure (EXAFS) analyses were performed using Athena and Artemis software packages.^[29] For XANES analyses, the spectra were normalized and

flattened. For EXAFS fitting, spectra were background subtracted, normalized, k^3 -weighted, and Fourier-transformed in the k range of $2.7\text{--}15.5 \text{ \AA}^{-1}$. EXAFS fitting was performed in k -space between 3 and 15 \AA^{-1} simultaneously on the k^1 -, k^2 -, and k^3 -weighted data.

In situ measurements were performed using a quartz capillary micro-reactor setup. (1 mm o.d., 20 μm thickness). The capillary was heated from below with a hot-air gas-blower (Oxford FMB). Gas flow rates (N_2 , H_2 , CO_2 , or a mixture of H_2 and CO_2) were maintained using Bronkhorst electronic mass flow controllers and the pressure was continuously monitored using a pressure gauge (Omega). The spectra were first measured under N_2 flow at 293 K. The gas flow was then switched to pure H_2 and the temperature was increased to 393 K (5 Kmin^{-1}). XANES measurements were performed continuously during the temperature ramp and EXAFS measurements were performed after reaching 393 K. After measurements in H_2 flow at 393 K, the gas flow was switched to CO_2 and XANES and EXAFS measurements were performed under CO_2 flow. Finally the gas flow was switched to a mixture of CO_2 and H_2 and the temperature was increased to 483 K (5 Kmin^{-1}). XANES measurements were performed continuously during the temperature ramp while spectra for EXAFS analysis were measured after reaching 483 K.

Synthesis of *N*-(3-Trimethoxysilylpropyl) Formamide functionalized Si/Pd

In a round bottom flask, 10 mL (3-Aminopropyl)trimethoxysilane (APTMS, 10.3 g, 57.5 mmol, 1 eq.) were cooled to 0°C . Over the next 5 min, 4 mL methyl formate were added dropwise. This mixture was stirred for 10 min, then heated to room temperature and stirred for an additional 4 h. Immediately afterwards, volatiles were removed at 1 mbar for 1.5 h to stop the reaction. Further purification was performed by heating the crude mixture in vacuum (95°C , 0.09 mbar) to remove any remaining APTMS. This yielded to 10.95 g (52.8 mmol, 92.0%) of a clear liquid containing the E- and Z-rotamers of the product in a ratio of 4:1

Amide functionalization was done by grafting with a 1:1 vol.-% mixture of a trimethoxysilane modified amine and anhydrous toluene. The amine content was controlled by the grafting procedure. After grafting, the particles are washed with ethanol ($1 \times 100 \text{ mL--}150 \text{ mL}$), iso-propanol ($1 \times 100 \text{ mL--}150 \text{ mL}$) and toluene ($1 \times 50 \text{ mL--}100 \text{ mL}$) are subsequently dried in vacuum at room temperature for 30 min and at 393 K for 3 h.

Acknowledgements

We would like to thank the Deutsche Forschungsgemeinschaft (DFG, German Research Foundation) for financial support via the priority programme SPP2080 (projects no. JE-260/13-1, GL 290/12-1, DE 659/13-1) We would like to thank Ch. Jandel for XPS measurements, M. Hahn for ^{29}Si MAS NMR measurements. The XAS measurements were performed at P65 beamline of DESY, Hamburg. The authors would like to acknowledge support from Dr. R. Khare (TUM), as well as Dr. Edmund Welter and other staff at the P65 beamlines at DESY, Hamburg. The TEM work was performed by D. Poppitz at the Institute of Chemical Technology, Universität Leipzig. Open Access funding enabled and organized by Projekt DEAL.

Conflict of Interest

The authors declare no conflict of interest.

Data Availability Statement

The data that support the findings of this study are available in the supplementary material of this article.

Keywords: amine · bifunctional · CO₂ capture and utilization · methanol · selective reduction

- [1] H. Naims, *Environmental Science and Pollution Research* **2016**, *23*, 22226–22241.
- [2] a) D. P. van Vuuren, A. F. Hof, M. A. E. van Sluisveld, K. Riahi, *Nat. Energy* **2017**, *2*, 902–904; b) K. Anderson, G. Peters, *Science* **2016**, *354*, 182–183; c) V. Masson-Delmotte, P. Zhai, A. Pirani, S. L. Connors, S. Berger, N. Caud, Y. Chen, L. Goldfarb, M. I. Gomis, M. Huang, K. Leitzell, E. Lonnoy, J. B. R. Matthews, T. K. Maycock, T. Waterfield, O. Yelekçi, R. Yu, B. Zhou, *Cambridge University Press* **2021**.
- [3] a) N. M. Rezayee, C. A. Huff, M. S. Sanford, *J. Am. Chem. Soc.* **2015**, *137*, 1028–1031; b) S. Kar, A. Goepfert, G. K. S. Prakash, *Acc. Chem. Res.* **2019**, *52*, 2892–2903; c) S. Kar, R. Sen, A. Goepfert, G. K. S. Prakash, *J. Am. Chem. Soc.* **2018**, *140*, 1580–1583; d) S. Kar, A. Goepfert, G. K. S. Prakash, *ChemSusChem* **2019**, *12*, 3172–3177; e) J. Kothandaraman, A. Goepfert, M. Czaun, G. A. Olah, G. K. S. Prakash, *J. Am. Chem. Soc.* **2016**, *138*, 778–781; f) J. Kothandaraman, J. Saavedra Lopez, Y. Jiang, E. D. Walter, S. D. Burton, R. A. Dagle, D. J. Heldebrant, *ChemSusChem* **2021**; n/a g) S. Kar, A. Goepfert, J. Kothandaraman, G. K. S. Prakash, *ACS Catal.* **2017**, *7*, 6347–6351; h) R. Sen, A. Goepfert, S. Kar, G. K. S. Prakash, *J. Am. Chem. Soc.* **2020**, *142*, 4544–4549; i) C. Reller, M. Pöge, A. Lißner, F. O. R. L. Mertens, *Environ. Sci. Technol.* **2014**, *48*, 14799–14804; j) M. Everett, D. F. Wass, *Chem. Commun.* **2017**, *53*, 9502–9504; k) J. B. Jakobsen, M. H. Rønne, K. Daasbjerg, T. Skrydstrup, *Angew. Chem. Int. Ed.* **2021**, *60*, 9174–9179; l) S.-T. Bai, G. De Smet, Y. Liao, R. Sun, C. Zhou, M. Beller, B. U. W. Maes, B. F. Sels, *Chem. Soc. Rev.* **2021**, *50*, 4259–4298; m) E. A. K. Wilson, S. C. Eady, T. Silbaugh, L. T. Thompson, M. A. Barteau, *J. Catal.* **2021**.
- [4] a) S. Wesselbaum, T. vom Stein, J. Klankermayer, W. Leitner, *Angew. Chem. Int. Ed.* **2012**, *51*, 7499–7502; *Angew. Chem.* **2012**, *124*, 7617–7620; b) D. A. Kuß, M. Hölscher, W. Leitner, *ChemCatChem* **2021**, *13*, 3319–3323.
- [5] C. A. Huff, M. S. Sanford, *J. Am. Chem. Soc.* **2011**, *133*, 18122–18125.
- [6] W. H. Bernskoetter, N. Hazari, *Acc. Chem. Res.* **2017**, *50*, 1049–1058.
- [7] a) S. Ghosh, A. Ghosh, S. Biswas, M. Sengupta, D. Roy, S. M. Islam, *ChemistrySelect* **2019**, *4*, 3961–3972; b) R. A. Molla, P. Bhanja, K. Ghosh, S. S. Islam, A. Bhaumik, S. M. Islam, *ChemCatChem* **2017**, *9*, 1939–1946; c) Y. Wang, B. Chen, S. Liu, X. Shen, S. Li, Y. Yang, H. Liu, B. Han, *ChemCatChem* **2018**, *10*, 5124–5127; d) Y. Zhang, H. Wang, H. Yuan, F. Shi, *ACS Sustainable Chem. Eng.* **2017**, *5*, 5758–5765; e) P. Ju, J. Chen, A. Chen, L. Chen, Y. Yu, *ACS Sustainable Chem. Eng.* **2017**, *5*, 2516–2528; f) Q. Zou, J. Chen, Y. Wang, J. Gu, F. Liu, T. Zhao, *ACS Sustainable Chem. Eng.* **2021**.
- [8] J. Kothandaraman, D. J. Heldebrant, *Green Chem.* **2020**, *22*, 828–834.
- [9] a) L. Artús Suárez, Z. Culakova, D. Balcells, W. H. Bernskoetter, O. Eisenstein, K. I. Goldberg, N. Hazari, M. Tilset, A. Nova, *ACS Catal.* **2018**, *8*, 8751–8762; b) L. Artús Suárez, U. Jayarathne, D. Balcells, W. H. Bernskoetter, N. Hazari, M. Jaraiz, A. Nova, *Chem. Sci.* **2020**, *11*, 2225–2230.
- [10] a) Y. Xie, P. Hu, T. Bendikov, D. Milstein, *Catalysis Science, Technology* **2018**, *8*, 2784–2788; b) T. Ikariya, K. Murata, R. Noyori, *Org. Biomol. Chem.* **2006**, *4*, 393–406; c) P. A. Dub, J. C. Gordon, *Nat. Chem. Rev.* **2018**, *2*, 396–408.
- [11] a) L. M. Martínez-Prieto, M. Puche, C. Cerezo-Navarrete, B. Chaudret, *J. Catal.* **2019**, *377*, 429–437; b) I. Cano, L. M. Martínez-Prieto, P. W. N. M. van Leeuwen, *Catalysis Science, Technology* **2021**, *11*, 1157–1185; c) M. Fang, R. A. Sánchez-Delgado, *J. Catal.* **2014**, *311*, 357–368; d) S. Wang, P. Zhou, L. Jiang, Z. Zhang, K. Deng, Y. Zhang, Y. Zhao, J. Li, S. Bottle, H. Zhu, *J. Catal.* **2018**, *368*, 207–216.
- [12] a) M. Tamura, S. Ishikawa, M. Betchaku, Y. Nakagawa, K. Tomishige, *Chem. Commun.* **2018**, *54*, 7503–7506; b) I. Sorribes, S. C. S. Lemos, S. Martín, A. Mayoral, R. C. Lima, J. Andrés, *Catalysis Science, Technology* **2019**, *9*, 6965–6976; c) R. A. Sánchez-Delgado, N. Machalaba, N. Ng-A-Qui, *Catal. Commun.* **2007**, *8*, 2115–2118.
- [13] K.-i. Shimizu, Y. Miyamoto, A. Satsuma, *J. Catal.* **2010**, *270*, 86–94.
- [14] J. Pazdera, E. Berger, J. A. Lercher, A. Jentys, *Catal. Commun.* **2021**, *159*, 106347.
- [15] a) V. Zelenák, M. Madaničová, D. Halamová, J. Čejka, A. Zukal, N. Murafa, G. Goerigk, *Chem. Eng. J.* **2008**, *144*, 336–342; b) F.-Y. Chang, K.-J. Chao, H.-H. Cheng, C.-S. Tan, *Sep. Purif. Technol.* **2009**, *70*, 87–95.
- [16] D. Zhao, J. Feng, Q. Huo, N. Melosh, H. Fredrickson Glenn, F. Chmelka Bradley, D. Stucky Galen, *Science* **1998**, *279*, 548–552.
- [17] P. F. Fulvio, S. Pikus, M. Jaroniec, *J. Mater. Chem.* **2005**, *15*, 5049–5053.
- [18] a) M. W. Hahn, M. Steib, A. Jentys, J. A. Lercher, *J. Phys. Chem. C* **2015**, *119*, 4126–4135; b) Z. Bacsik, N. Ahlsten, A. Ziadi, G. Zhao, A. E. Garcia-Bennett, B. Martin-Matute, N. Hedin, *Langmuir* **2011**, *27*, 11118–11128.
- [19] a) R. B. Said, J. M. Kolle, K. Essalah, B. Tangour, A. Sayari, *ACS Omega* **2020**, *5*, 26125–26133; b) B. Aziz, N. Hedin, Z. Bacsik, *Microporous Mesoporous Mater.* **2012**, *159*, 42–49.
- [20] a) K. P. Battjes, A. M. Barolo, P. Dreyfuss, *J. Adhes. Sci. Technol.* **1991**, *5*, 785–799; b) Z. Bacsik, R. Atluri, A. E. Garcia-Bennett, N. Hedin, *Langmuir* **2010**, *26*, 10013–10024; c) N. Hedin, Z. Bacsik, *Current Opinion in Green and Sustainable Chemistry* **2019**, *16*, 13–19; d) K. Li, J. D. Kress, D. S. Mebane, *J. Phys. Chem. C* **2016**, *120*, 23683–23691; e) A. Danon, P. C. Stair, E. Weitz, *J. Phys. Chem. C* **2011**, *115*, 11540–11549.
- [21] T. Watabe, K. Yogo, *Sep. Purif. Technol.* **2013**, *120*, 20–23.
- [22] a) J. T. Moulder, W. F. Stickle, P. E. Skobol, K. D. Bomben, *Handbook of X-ray Photoelectron Spectroscopy*, Perkin-Elmer Corp., **1992**; b) C. D. Wagner, A. V. Naumkin, A. Kraut-Vass, J. W. Allison, C. J. Powell, J. R. Rumble Jr., NIST X-ray Photoelectron Spectroscopy Database. **2021**.
- [23] a) S. Masuda, K. Mori, Y. Futamura, H. Yamashita, *ACS Catal.* **2018**, *8*, 2277–2285; b) M.-H. Jin, J.-H. Park, D. Oh, J.-S. Park, K.-Y. Lee, D.-W. Lee, *Int. J. Hydrogen Energy* **2019**, *44*, 4737–4744.
- [24] N. Graf, E. Yegen, T. Gross, A. Lippitz, W. Weigel, S. Krakert, A. Terfort, W. E. S. Unger, *Surf. Sci.* **2009**, *603*, 2849–2860.
- [25] J. R. Cabrero-Antonino, R. Adam, V. Papa, M. Beller, *Nat. Commun.* **2020**, *11*, 3893.
- [26] J. Wang, C. Zhou, Z. Gao, X. Feng, Y. Yamamoto, M. Bao, *ChemCatChem* **2021**, *13*, 2702–2708.
- [27] T. Neveux, H. Hagi, Y. Le Moullec, *Energy Procedia* **2014**, *63*, 463–470.
- [28] E. Welter, R. Chernikov, M. Herrmann, R. Nemausat, *AIP Conf. Proc.* **2019**, *2054*, 040002.
- [29] N. M. B. Ravel, *J. Synchrotron Radiat.* **2005**, *4*, 537–541.

Manuscript received: May 13, 2022
Revised manuscript received: July 19, 2022
Accepted manuscript online: July 20, 2022
Version of record online: August 30, 2022